RSC Advances

PAPER

View Article Online
View Journal | View Issue

Open Access Article. Published on 22 May 2021. Downloaded on 12/5/2025 7:07:59 PM.
This article is licensed under a Creative Commons Attribution-NonCommercial 3.0 Unported Licence.

Check for updates

Cite this: *RSC Adv.*, 2021, **11**, 18525

Peroxymonosulfate activation by tea residue biochar loaded with Fe_3O_4 for the degradation of tetracycline hydrochloride: performance and reaction mechanism

Qirui Wang, Yixuan Shi, Shiyi Lv, Ying Liang and Pengfei Xiao *

The recycling of agricultural and food waste is an effective way to reduce resource waste and ameliorate the shortage of natural resources. The treatment of antibiotic wastewater is a current research hotspot. In this study, waste tea residue was used as a raw material to prepare biochar (T-BC) and loaded with Fe_3O_4 as a catalyst to activate peroxymonosulfate (PMS) for oxidative degradation of tetracycline hydrochloride (TCH). Analysis techniques such as BET, SEM, XRD, FT-IR, XPS and VSM indicated that the heterogeneous catalyst (Fe_3O_4@T-BC) with good surface properties and magnetic properties was successfully prepared. The results of batch-scale experiments illustrated that when the dose of the Fe_3O_4@T-BC catalyst was 1 g L^{-1}, the concentration of PMS was 1 g L^{-1}, and the initial pH was 7, the degradation rate of TCH with a concentration of 50 mg L^{-1} reached 97.89% after 60 minutes of reaction. When the initial pH was 11, the degradation rate of TCH reached 99.86%. After the catalyst was recycled four times using an external magnet, the degradation rate of TCH could still reach 71.32%. The data of removal of TCH could be best fitted by a pseudo-first-order model. The analysis of the degradation mechanism through a free radical quenching experiment and EPR analysis, as well as the exploration of TCH intermediate products and reaction paths through the LC-MS method, all confirmed that the Fe_3O_4@T-BC prepared by this method is expected to become a cost-effective and environmentally friendly heterogeneous catalyst for activating persulfate degradation of tetracycline antibiotics.

Received 2nd March 2021
Accepted 17th May 2021

DOI: 10.1039/d1ra01640g

rsc.li/rsc-advances

1. Introduction

Because of the deterioration of the ecological environment and the shortage of natural resources, the recycling of agricultural and food waste has received extensive attention in the reduction of wasting resources and saving material costs.[1] Tea is the second most popular beverage in the world, and its consumption is second only after water. As a significant tea-drinking country, China's tea consumption is among the highest in the world, and national tea production reached more than 2.8 million tons in 2019.[2] With the rapid development of the tea industry, a large amount of waste tea residue is generated every year, most of which is treated and disposed of as waste, resulting in a large waste of resources. Therefore, it is urgent to explore new ways to make tea dregs fully utilized. Recently, the use of tea dregs as a raw material to make biochar has become an important method for its resource utilization,[3] and its applications in the environmental field have gradually increased.[4] However, most of these applications rely on its adsorption capacity as an adsorbent to remove heavy metal ions,[5] inorganic pollutant ions,[6] and organic pollutants[7] in wastewater. There are few studies on using tea residue biochar as a carrier of metal oxides to activate persulfate to degrade organic pollutants synergistically.

Antibiotics used to treat various bacterial and pathogen infections are widely used in livestock and poultry breeding and pharmaceutical industries. They have a wide variety and complex structure, and difficult to degrade.[8] The potential toxicity, teratogenicity and genotoxicity of antibiotics remaining in the aquatic environment to humans and aquatic organisms have attracted widespread attention as severe environmental concerns.[9] Among them, tetracycline antibiotics are broad-spectrum antibiotics widely present in the environment and have the highest detection frequency. The long-term accumulation of tetracyclines can inhibit the development of young children and bone growth and seriously endanger human health.[10] Therefore, it is vital to find a green and efficient way to control antibiotic pollution in the water environment.

At present, the methods for removing antibiotic pollutants in wastewater include adsorption,[11] biological, ion exchange, photocatalysis,[12] and advanced oxidation. In the adsorption method, the number of regeneration and utilization of the adsorbent cannot be guaranteed. The photocatalytic method

College of Forestry, Northeast Forestry University, Harbin 150040, China. E-mail: xpfawd@nefu.edu.cn

© 2021 The Author(s). Published by the Royal Society of Chemistry

Open Access Article. Published on 22 May 2021. Downloaded on 12/5/2025 7:07:59 PM.
This article is licensed under a Creative Commons Attribution-NonCommercial 3.0 Unported Licence.

requires high light transmittance of the photocatalyst, light source and water quality, which leads to poor practical application effects.[13] The ion exchange method has low current efficiency, high operating costs, and secondary pollution. By contrast, based on sulfate radicals, the advanced oxidation method can decompose difficult-to-degrade organic pollutants into CO_2, H_2O and other small molecule compounds in a short period of time under the condition of neutral pH at normal temperature and pressure.[14] Because of its high efficiency and thoroughness, simple process and lack of secondary pollution, it has received extensive attention from researchers and has broad application prospects in the field of water treatment and groundwater remediation.[15] This method mainly activates peroxymonosulfate (PMS) or peroxodisulfate (PDS) through transition metal ions, high temperature, ultraviolet light or ultrasonic irradiation to produce $SO_4^{-\bullet}$, which with a strong oxidizing ability (redox potential of approximately 2.5–3.1 V) to remove organic pollutants.[16] Compared with PDS with steric hindrance, the non-polar PMS with asymmetric molecular structure is more susceptible to attack by nucleophiles and more easily activated.[17] And PMS will generate SO_4^{2-} after its oxidation, which causes little harm to the water environment. Among the activation methods, the use of external energy such as ultrasonic and ultraviolet activation is an effective method, but the high energy consumption in the process and harsh reaction conditions hinder its large-scale application.[17] Transition metals and their oxides have better activation efficiency and can be conducted with simple operation under normal temperature and pressure.[18] However, due to the small particle size and high surface energy, nano metal oxides, especially magnetic particles such as Fe_3O_4, are prone to agglomeration and ion leaching to cause secondary pollution problems, limiting their application in practice.[17] The preparation of nanometer iron oxide composite materials using porous materials as the carrier,[18] can improve the dispersibility and reactivity of nanometer iron oxides and can utilize the synergistic effect of iron oxide and carrier materials to improve the removal effect of pollutants.[19,20] Among them, carbon materials have shown broad application prospects in the field of catalysis by virtue of their unique nanostructure, excellent conductivity, chemical stability and adsorption characteristics. Using carbon materials as a carrier can also promote adsorption and cooperate with metal oxides to activate PMS, showing a higher activation effect.

In this study, tea residue biochar (T-BC) was prepared by high-temperature pyrolysis method using tea residue as raw material, and a series of heterogeneous catalysts (Fe_3O_4@T-BC) with different percentage loading of Fe_3O_4 were prepared by the impregnation–coprecipitation method. With tetracycline hydrochloride (TCH) as the target pollutant, Fe_3O_4@T-BC is used as an activator to activate peroxymonosulfate to degrade TCH oxidatively. The catalyst materials were tested and evaluated, including surface morphology, crystal structure, phase composition, and recycling characteristics. To find the best degradation conditions for TCH, the effects of various parameters, such as catalyst dosage, initial TCH concentration, PMS concentration, initial pH, and inorganic anions, on the degradation effect of tetracycline were explored. More importantly, in order to further confirm the superiority of the application of the catalyst Fe_3O_4@T-BC prepared in this research in activating PMS to degrade TCH, the following research is also conducted: first, through free radical quenching experiment and EPR analysis aimed to determine the activated species and participating mechanisms. Second, by using LC-MS to analyze the intermediate products, this research also discussed the possible reaction pathways and mechanism of action of the catalytic degradation system. Third, the reusability of the catalyst was studied. This research is expected to provide a scientific basis and theoretical support for the further application of this technology in antibiotic wastewater treatment.

2. Experimental

2.1 Chemicals and reagents

Tetracycline hydrochloride ($C_{22}H_{25}N_2O_8Cl$, 96%), potassium monopersulfate ($KHSO_5 \cdot 0.5KHSO_4 \cdot 0.5K_2SO_4$, ≥42% $KHSO_5$ basis), sodium hydroxide (NaOH, 96%), ethanol (EtOH, AR, ≥99.5%), *tert*-butanol (TBA, GR, ≥99.5%), furfuryl alcohol (FFA, CP, 97%), *p*-benzoquinone (*p*-BQ, 99%), ferric chloride ($FeCl_3 \cdot 6H_2O$, AR, 99%), ferrous sulfate ($FeSO_4 \cdot 7H_2O$, AR, 99%), sodium carbonate (Na_2CO_3, 99.8%), sodium sulfate (Na_2SO_4, AR, 99%), sodium chloride (NaCl, 99.5%), sodium bicarbonate ($NaHCO_3$, 99.5%) and sodium acetate (CH_3COONa, AR) were purchased from Aladdin Shanghai. In the experimental process, all the reagents were analytically pure, and the water for dilution and dissolution was ultrapure water.

2.2 Preparation of catalysts

The feedstock for catalyst preparation was tea residues (the tea leaf that was used) collected from the Northeast Forestry University campus drink shops. After being washed with ultrapure water several times, the clean tea residues were dried at 60 °C in an oven. Then, the dry tea residues were pyrolyzed at 500 °C in a muffle furnace under oxygen-limited conditions with a retention time of 2 h, ground with a mortar and passed through a 100-mesh sieve. Finally, the biochar was washed with ultrapure water several times to remove ash produced by pyrolysis, dried at 60 °C for 12 h and labeled T-BC.

Using T-BC as the raw material, iron oxide-modified biochar of origin was prepared by the impregnation–coprecipitation method. The synthesis procedure of Fe_3O_4@T-BC was described as follows: 2 g T-BC was dispersed into 30 mL ultrapure water and placed in a magnetic stirrer. Next, 10 mL mixed solutions containing 0.25 M $FeSO_4 \cdot 7H_2O$ and 0.5 M $FeCl_3 \cdot 6H_2O$ (volume ratio of 1 : 1) were rapidly added into the above solution. After being sealed, the mixture was stirred evenly and then soaked for 0.5 h. Afterwards, 5 M NaOH was added dropwise at a constant speed into the mixture until the pH rose to approximately 10–11 with a black precipitate generated. Stir for another 1 h before setting for approximately 2 h at 80 °C. Finally, the black solid was separated and washed with ultrapure water until a neutral pH was achieved, dried at 60 °C for 12 h and stored in an airtight container.

 © 2021 The Author(s). Published by the Royal Society of Chemistry

Open Access Article. Published on 22 May 2021. Downloaded on 12/5/2025 7:07:59 PM.
This article is licensed under a Creative Commons Attribution-NonCommercial 3.0 Unported Licence.

2.3 Experimental procedures

In all batch trials, the TCH removal experiments were conducted in a series of 100 mL conical flasks. Fifty milliliters of PMS solution was placed in a flask containing 50 mL of TCH solution, then the catalyst (Fe_3O_4@T-BC) was rapidly added to the reactors, and the glass vials were capped tightly. The conical flasks were placed in a thermostatic air bath shaker at 25 °C to initiate the reaction. During the reaction, 3 mL of sample supernatant was filtered through a 0.45 μm filter into a cuvette every 10 min, and the supernatant was immediately analyzed to determine the residual TCH concentration using a UV-Vis spectrophotometer at 357 nm.[14] Single-variable control trials were carried out to research and optimize the removal conditions, including initial pH (3.0–11.0), initial TCH concentration (25–100 mg L^{-1}), PMS concentration (0.5–2.0 g L^{-1}), Fe_3O_4@T-BC dosage (0.2–1.0 g L^{-1}) and reaction time (0–60 min). The initial solution pH was adjusted with 0.1 M HCl or 0.1 M NaOH. The experiments with catalyst and PMS were set as the blank.

In the free radical quenching experiments, EtOH was used to quench both $SO_4^{-\bullet}$ and $^{\bullet}OH$.[21] TBA was used to quench $^{\bullet}OH$.[22] FFA was used to quench $^1O_2$.[23] *p*-BQ was used to quench $^{\bullet}O_2^-$.[24] In the experiment, TCH solution, Fe_3O_4@T-BC, quencher (ethanol, *tert*-butanol, furfuryl alcohol or *p*-benzoquinone) and PMS solution were sequentially added to the conical flask. The conditions for each test were controlled as follows: system volume = 100 mL, [TCH] = 50 mg L^{-1}, Fe_3O_4@T-BC dosage = 1 g L^{-1}, [PMS] = 1 g L^{-1}, quencher concentration = 50 mM, and reaction time = 1 h. During the reaction, samples were taken after every 10 minutes to determine the remaining TCH concentration. All reaction tests were repeated three times, and the average of the obtained results was taken for data analysis.

2.4 Analytical methods

The degradation solution of TCH was determined by UV-1800 (Mapada, China) and TU-1901 (PERSEE, China) UV-Vis spectrophotometry. Using ASAP 2460 series automatic fast physical adsorption analyzer (Micromeritics, China), the surface area, pore volume and pore size of T-BC and Fe_3O_4@T-BC were analyzed. The microscopic surface morphology and loading status of Fe_3O_4@T-BC were recorded by a su8020 field emission scanning electron microscope (SEM) (Hitachi, Japan). The microscope was coupled to a HORIBA EX250 energy dispersive spectroscopy (EDS) detector (HORIBA, Japan) for elemental analysis. The X-ray diffraction (XRD) patterns of T-BC and Fe_3O_4@T-BC were recorded by a TD-3500 *in situ* reaction X-ray powder diffractometer (Tongda, China). Use X-ray photoelectron spectrometer (XPS) (Thermo Fisher, US) to analyze the elemental composition of materials. Chemical characterizations of T-BC and Fe_3O_4@T-BC were carried out using iS10 FT-IR spectrometer Fourier transform infrared spectrophotometer (FT-IR) (Nicolet, US). The magnetic properties of the material are tested with the MPMS-3 magnetic measurement system (VSM) (Quantum Design, US). The electron paramagnetic resonance spectra of trapped radicals were obtained by an A300-10/12 electron paramagnetic resonance device (EPR) (Bruker, Germany), which used 5,5-dimethyl-1-pyrroline N-oxide (DMPO) and 2,2,6,6-tetramethyl-4-piperidine (TEMP) as the radical spin-trapping agents to identify the radicals generated from the Fe_3O_4@T-BC/PMS system. The concentration of leached iron was measured by a UV-1800 spectrophotometer at 510 nm using the 1,10-phenanthroline method. The LC-MS analysis was carried by an Ultimate 3000 UPLC with Thermo Scientific Q Exactive mass spectrometer (Thermo Fisher, US). The mineralization of TCH was determined by total organic carbon (TOC) using a TOC-L CPN analyzer (Shimadzu, Japan).

3. Results and discussion

3.1 Characterization of Fe_3O_4@T-BC

3.1.1 Pore properties and specific surface area analysis. Compared with T-BC, the BET specific surface area, total pore volume, average pore diameter, and the *t*-plot external surface area of Fe_3O_4@T-BC are significantly increased while the *t*-plot micropore area is significantly reduced. The BET specific surface area increased from 92.34 to 97.41 m^2 g^{-1}, the total pore volume increased from 0.052 to 0.098 m^2 g^{-1}, the external surface area increased from 21.04 to 40.51 m^2 g^{-1}, the average pore size increased from 2.23 to 4.04 nm, and the micropore area decreased from 71.30 to 56.90 m^2 g^{-1}. These fully demonstrated that the Fe_3O_4@T-BC prepared by this method successfully loaded Fe_3O_4 on the surface of T-BC, greatly enlarged the specific surface area of the catalyst material, and blocked the pores of the T-BC to a lesser degree. Combined with the analysis of the average pore size, the catalyst material is a mesoporous material with good surface properties. The N_2 adsorption isotherms of T-BC and Fe_3O_4@T-BC belong to IUPAC type-I isotherms and type-II isotherms, respectively, showing the adsorption characteristics of micropores and mesopores, which is consistent with the pore size distribution.

3.1.2 Surface topography analysis. The modified biochar (Fe_3O_4@T-BC) was analyzed by SEM to observe the microscopic surface morphology and loading status. Fig. 1a and b are the field emission scanning electron micrographs of Fe_3O_4@T-BC at 20k and 60k magnifications. As illustrated in Fig. 1a and b, Fe_3O_4 particles existed in the spheroid state, and most of the particles of 100–200 nm could be seen in the figure, which were slightly aggregated owing to the magnetic effect. However, most agglomerated particles were still tiny. It can also be seen that the surface of Fe_3O_4@T-BC is rough and has a developed pore structure. Fe_3O_4 is evenly loaded on the pore surface of T-BC, indicating that the T-BC carrier plays a role in dispersing Fe_3O_4, improves the catalytic degradation reaction and can increase the number of active sites for the catalytic degradation reaction, thereby improving its catalytic performance. In addition, Fig. 1c shows the field emission scanning electron micrographs of Fe_3O_4@T-BC after participating in a catalytic degradation reaction. By comparing the images of Fe_3O_4@T-BC before and after participating in the catalytic degradation reaction, it can be seen that Fe_3O_4 particles after the catalytic reaction are more evenly and finely distributed on the surface of T-BC, and needle-like structured substances appeared, indicating that the reaction site occurs on the surface of the catalyst,

Open Access Article. Published on 22 May 2021. Downloaded on 12/5/2025 7:07:59 PM.
This article is licensed under a Creative Commons Attribution-NonCommercial 3.0 Unported Licence.

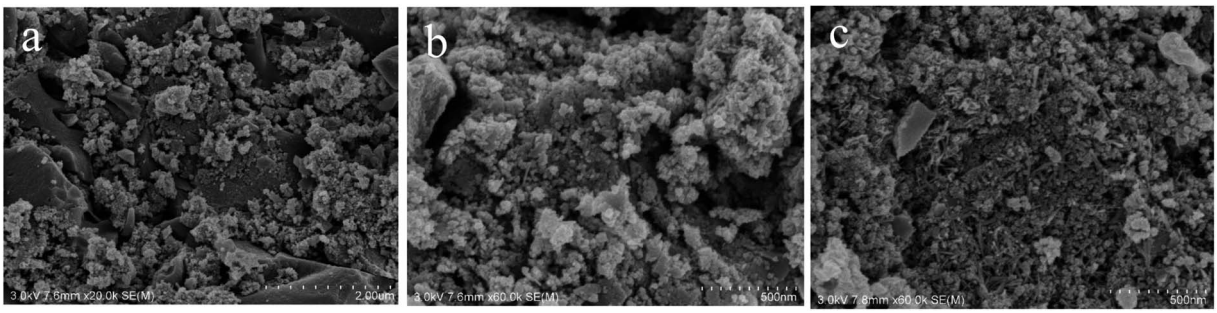

Fig. 1 SEM images of Fe_3O_4@T-BC before (a and b) and after (c) reaction.

and the Fe_3O_4 involved in the reaction reattached to the surface of the biochar after the reaction.

3.1.3 Phase structure and element composition analysis. X-ray diffraction technology (XRD) was utilized to explore the crystal structure and phase composition of T-BC and Fe_3O_4@T-BC. Fig. 2a shows that there is a broad peak of $2\theta = 18.5$–$30.5°$ in the XRD pattern of T-BC, which is caused by the amorphous structure of graphite in biochar. Fe_3O_4@T-BC has obvious diffraction peaks with 2 theta values of 35.5°, 43.2°, 57.3° and 62.7°,[20] which can match well with the standard card of PDF# 88-0315. This preliminarily shows that the metal oxide contained in the synthesized Fe_3O_4@T-BC is Fe_3O_4. The black precipitates observed in the material preparation experiment and the Fe_3O_4@T-BC powder can be attracted by the magnet, both of which indicated that Fe_3O_4 particles were successfully and evenly loaded on the surface of T-BC. And comparing curve 2 and curve 3, it can be found that the X-ray diffraction patterns of Fe_3O_4@T-BC catalyst before and after the reaction are not significantly different, which indicates that the catalyst material has good stability.

Fig. 2b shows the XPS spectrum of Fe_3O_4@T-BC catalyst material. It can be seen from the figure that the sample contains Fe, C and O elements, and the binding energy of Fe at 711.08 eV and 725.08 eV can be confirmed as Fe $2p_{3/2}$ and Fe $2p_{1/2}$ of Fe_3O_4. This is consistent with Mashesh's research conclusion.[25] The peak at 284.8 eV, 530.17 eV and 711.05 eV assigned to C 1s, O 1s and Fe 2p, accounted for 43.57%, 38.53% and 17.9%, respectively.

3.1.4 Chemical structure analysis. The FT-IR spectrum (Fig. 3a) showed a broad peak at 3421.26 cm^{-1}, representing –OH stretching, which was attributed to interlayer crystal water or hydroxyl groups in the tea in Fe_3O_4@T-BC.[26] Compared with T-BC, the position of the Fe_3O_4@T-BC functional group was blue shifted, and the absorption peak was weakened, indicating that the number of hydroxyl groups in biochar decreased during the negative magnetic process.[27] The peaks at 879.90 cm^{-1} and 1057 cm^{-1}, were due to the tensile vibrations of C–H and C–O out of plane vibrations respectively.[28] A peak related to the C–O vibration of the oxygen atom was found at 1166.38 cm^{-1}. The peaks at 1591.54 cm^{-1} were probably because of C=O bond stretching.[29] The peak at 594.05 cm^{-1} showed the presence of O–S in the infrared spectrum of T-BC, which can also be seen in the infrared spectrum of Fe_3O_4@T-BC.[30] In addition, the difference between Fe_3O_4@T-BC and T-BC is that there is a strong Fe–O absorption peak at 579.02 cm^{-1},[27] which indirectly proves that Fe_3O_4 was successfully synthesized on the biochar. Studies have shown that these oxygen-containing functional groups on the surface of carbon materials can directly act as catalytic sites or intermediates for electron transfer to affect the catalytic activity of biochar. First, oxygen-containing functional groups directly act as catalytic sites to activate PMS and promote pollutant degradation.[31] Secondly, oxygen-containing functional groups also can be used as an electronic medium to promote the degradation of pollutants.[32] In addition, oxygen-containing functional groups can also affect its catalytic activity by regulating the conductivity or surface charge of biochar.[33] The FT-IR spectrum (Fig. 3a) also compares the infrared spectra before and after Fe_3O_4@T-BC is used. The absorption peak decreases after four cycles of Fe_3O_4@T-BC. In addition, after Fe_3O_4@T-BC participates in the catalytic degradation reaction, there is still an Fe–O absorption peak at 581.43 cm^{-1} in the infrared spectrum, which indicates that the Fe_3O_4 on the surface has not fallen off after Fe_3O_4@T-BC is used.

3.1.5 Magnetic performance analysis. The saturation magnetization of the material is a key parameter for achieving magnetic separation. The magnetic properties of Fe_3O_4@T-BC catalysts were evaluated under magnetic field cycles between −20 000 and +20 000 Oe at 298 K. Fig. 3b shows the magnetization curve of Fe_3O_4@T-BC. The curve does not show hysteresis effect and coercivity at room temperature, indicating that Fe_3O_4@T-BC is a superparamagnetic material with a saturation magnetization of 44.64 emu g^{-1}. It is learned from the literature that the saturation magnetization of pure Fe_3O_4 particles is about 68.4 emu g^{-1}, which is higher than the Fe_3O_4@T-BC prepared in this research. It may be due to the presence of non-magnetic T-BC in Fe_3O_4@T-BC. Studies have found that when the saturation magnetization exceeds 16.3 emu g^{-1}, magnetic separation can be achieved by conventional magnetic separation.[34] Therefore, the prepared magnetic catalyst material can be easily separated from solid and liquid by magnetic separation after participating in the reaction, and the recovery rate of the catalyst can be improved. Experiments have also found that when there is a permanent magnet nearby, Fe_3O_4@T-BC still exhibits a strong magnetic response, which

 © 2021 The Author(s). Published by the Royal Society of Chemistry

Open Access Article. Published on 22 May 2021. Downloaded on 12/5/2025 7:07:59 PM.
This article is licensed under a Creative Commons Attribution-NonCommercial 3.0 Unported Licence.

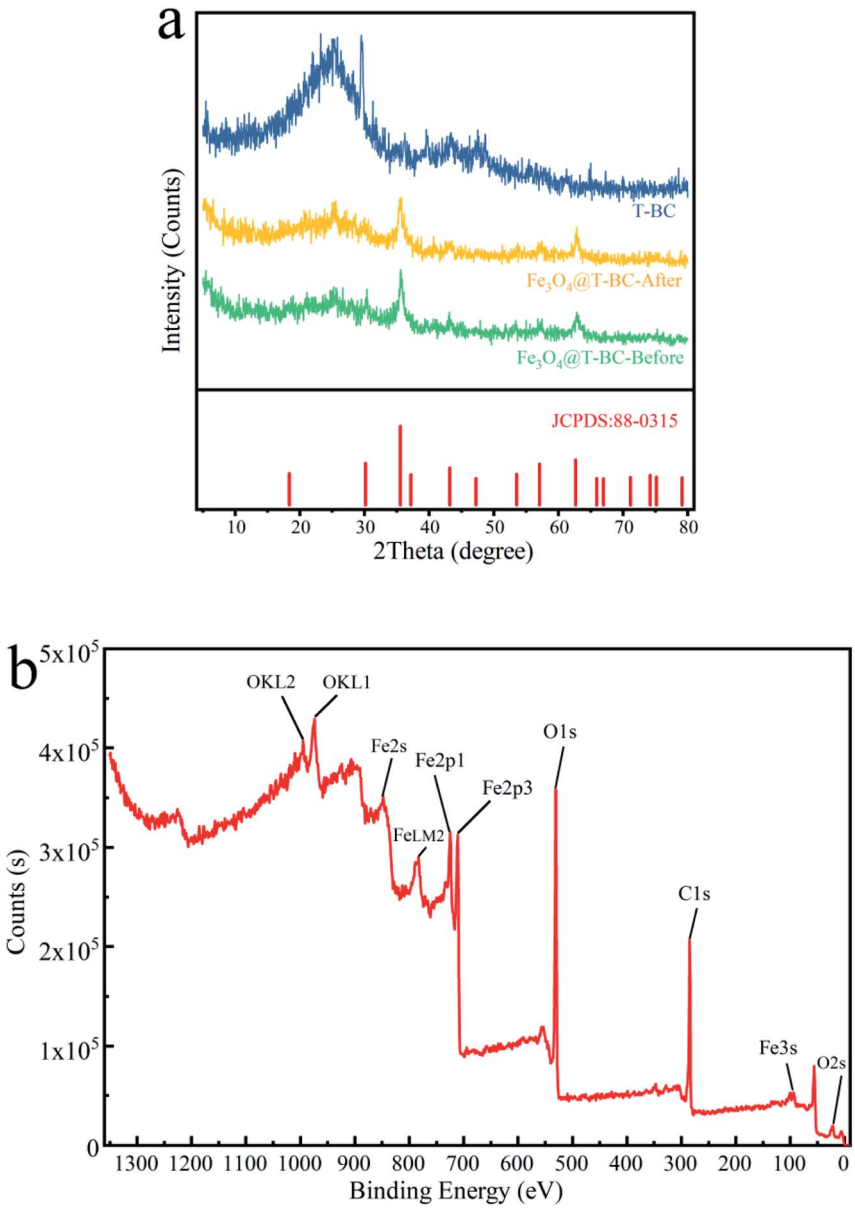

Fig. 2 XRD analysis of T-BC and Fe_3O_4@T-BC (a); XPS analysis of Fe_3O_4@T-BC (b).

indicates that Fe_3O_4@T-BC catalyst can be recycled, reduce the cost of use, and has the potential for practical application.

3.2 Degradation of TCH in different systems

Initial assays were performed with TCH as the model compound in aqueous solution. Fig. 4 presents (1) the adsorption of TCH by Fe_3O_4@T-BC, (2) the degradation of TCH by PMS alone, (3) the degradation of TCH by PMS in the presence of T-BC, and (4) the degradation of TCH by PMS in the presence of Fe_3O_4@T-BC. The removal rate of TCH under only the Fe_3O_4@T-BC system reached 56.95% within 60 min. This adsorption is attributed to the loose and porous structure of Fe_3O_4@T-BC. However, the results showed that the TCH concentration decreased significantly only in the first ten minutes of the reaction, and there was no significant change in the TCH concentration after 30 minutes. According to Li B.,[35] the reason is that the adsorption capability of Fe_3O_4@T-BC decreases with the increase of TCH adsorbed on Fe_3O_4@T-BC, and reaches adsorption saturation after 30 minutes of reaction. Only 58.89% of TCH was removed by PMS alone, which was in accordance with a previous study showing that PMS is not reactive obviously without certain activation for the degradation of tetracycline. This phenomenon was also observed in previous research.[36,37] On the other hand, 68.35% of tetracycline was removed by PMS in the presence of T-BC. This adsorption is attributed to T-BC activating the degradation of TCH by persulfate. Under identical conditions, 93.50% removal of TCH could be achieved by the Fe_3O_4@T-BC/PMS system, and the degradation rate was as high as 75.50% in the first ten minutes of the reaction. This phenomenon was better compared with F. Shao's study, in which the highest

Open Access Article. Published on 22 May 2021. Downloaded on 12/5/2025 7:07:59 PM.
This article is licensed under a Creative Commons Attribution-NonCommercial 3.0 Unported Licence.

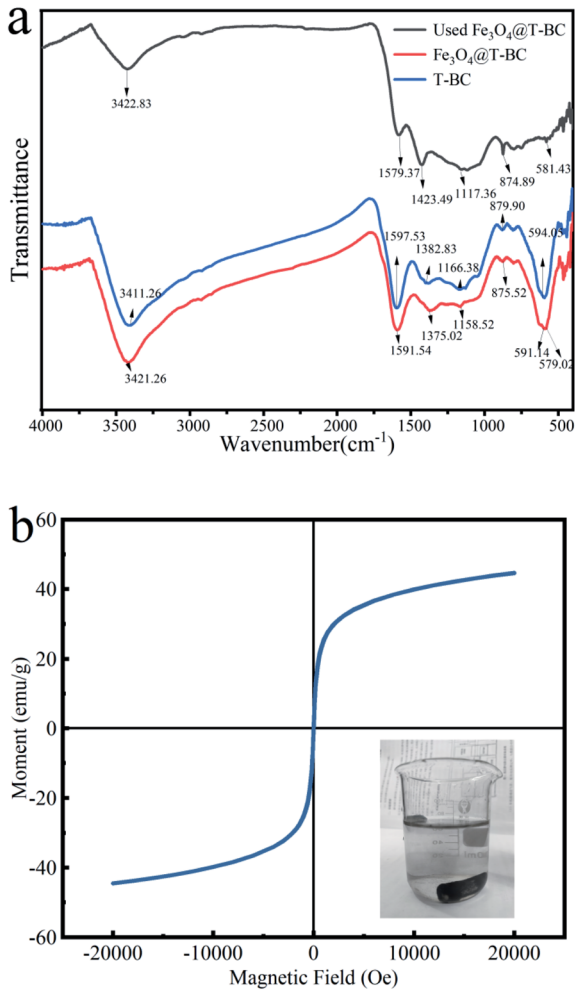

Fig. 3 FTIR analysis of Fe_3O_4@T-BC (a); VSM analysis of Fe_3O_4@T-BC (b).

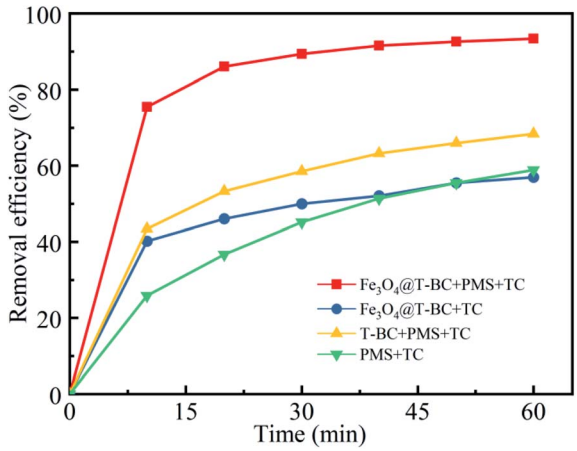

Fig. 4 Degradation of TCH in different systems.

removal efficiency was 87.58% by the nFe(0)/BC-PS system.[16] The results show that the degradation rate of TCH by the Fe_3O_4@T-BC/PMS system is not only much higher than that of the other three systems but also faster than that of the other three systems.

3.3 Experimental condition optimization

3.3.1 Effect of percentage loading of Fe_3O_4. In order to explore the effect of percentage loading of Fe_3O_4 on degradation of TCH, by controlling the amount of reagents, biochar materials with Fe_3O_4 content of 5 wt%, 10 wt%, 20 wt% and 30 wt% were prepared. Test under the conditions of the dose of the Fe_3O_4@T-BC catalyst was 1 g L^{-1}, the concentration of PMS was 1 g L^{-1}, and the concentration of TCH was 50 mg L^{-1}. The result is shown in Fig. 5a. After 60 minutes of reaction, the composite carbon material loaded with Fe_3O_4 has a significantly higher degradation rate than pure T-BC deactivated PMS to degrade TCH. And the degradation rate of Fe_3O_4@T-BC with a loading of 10 wt% is the largest, which is 93.25%. Compared with the original biochar, the removal rate of TCH is increased by 52.84%. The degradation rate of Fe_3O_4@T-BC (30 wt%) with the largest loading amount is significantly lower than other loadings of Fe_3O_4@T-BC in initial 10 min before of the reaction. It may be due to the high loading that Fe_3O_4 particles blocked the pores of the biochar, thereby reducing the surface area of the biochar and reducing the adsorption of TCH by the oxygen-containing groups of the biochar in the early stage of the reaction. The degradation efficiency of Fe_3O_4@T-BC with loadings of 10 wt% and 20 wt% was the largest at the initial stage of the reaction, and the removal rate of TCH was also higher after 60 min. Therefore, it is concluded that Fe_3O_4@T-BC with Fe_3O_4 loading between 10–20 wt% has the best effect on activating PMS to degrade TCH. In the subsequent exploratory experiments, high-quality composite carbon materials with a loading amount in this range are used as catalysts.

3.3.2 Effect of Fe_3O_4@T-BC dosage. After 60 min, with the addition of Fe_3O_4@T-BC increasing from 0.2 g L^{-1} to 1.0 g L^{-1}, the degradation rate continuously increased from 74.41% to 90.41%. As shown in Fig. 5b, the degradation rate of TCH increases sequentially with increasing dosage of Fe_3O_4@T-BC.[38] These findings were in good agreement with previous studies that the degradation efficiency of activated persulfate continuously increases because the increase in Fe_3O_4@T-BC dosage might provide more $SO_4^{-\bullet}$ in the activated system to participate and accelerate the degradation of TCH.[39]

3.3.3 Effect of PMS concentration. Similarly, the degradation of TCH as the PMS concentration increased from 0.5 g L^{-1} to 2.0 g L^{-1} was studied (Fig. 5c). After 10 min, the degradation rate of TCH with 2.0 g L^{-1} PMS was significantly increased to 62.19%, which is nearly 1.5 times higher than that of the 0.5 g L^{-1} PMS system. According to Ma D.,[40] the degradation of TCH increases when the PMS dosages are increased. This may be interpreted as generating more $SO_4^{-\bullet}$ in the activated system[41] and increasing the frequency of contact between tetracycline hydrochloride molecules and $SO_4^{-\bullet}$.[42] This phenomenon was also observed in previous research. However, when the PMS dosage increases to 2.0 g L^{-1}, the degradation rate is 90.65%, and the degradation rate shows a downward trend. It was similar to Z. Li, in which the degradation efficiency of TCH

 © 2021 The Author(s). Published by the Royal Society of Chemistry

Open Access Article. Published on 22 May 2021. Downloaded on 12/5/2025 7:07:59 PM.
This article is licensed under a Creative Commons Attribution-NonCommercial 3.0 Unported Licence.

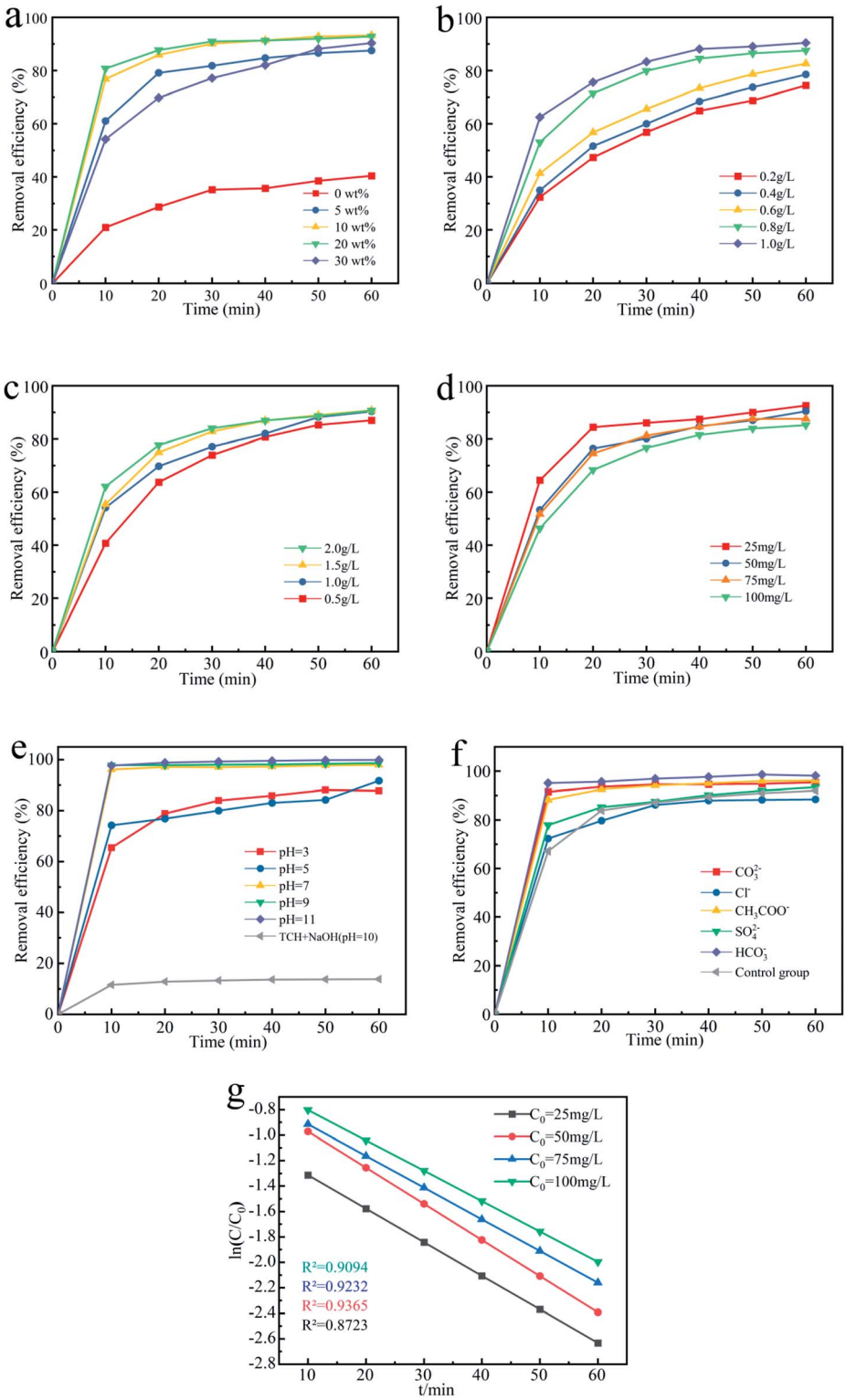

Fig. 5 (a) Effect of percentage loading of Fe_3O_4; (b) effects of Fe_3O_4@T-BC dosage; (c) effect of PMS concentration; (d) effect of TCH concentration; (e) effect of initial solution pH; (f) effect of coexisting ions (g) effect of TCH concentration and kinetic curves on the removal efficiency of TCH in the Fe_3O_4@T-BC/PMS system.

slightly decreased when the PMS concentration increased.[43] It can be seen that the increase in the amount of PMS does not keep the degradation rate increasing; in contrast, the generated excess $SO_4^{-\bullet}$ leads the free radicals to annihilate each other and reduces the degradation rate. These findings were in good agreement with previous studies.[44,45]

Open Access Article. Published on 22 May 2021. Downloaded on 12/5/2025 7:07:59 PM. This article is licensed under a Creative Commons Attribution-NonCommercial 3.0 Unported Licence.

3.3.4 Effect of initial TCH concentration. The effect of different initial concentrations of TCH on the degradation effect is shown in Fig. 5d. When the initial TCH concentration was 25 mg L^{-1}, the degradation rate reached 88.44% after 20 min, which was 20.01% higher than the initial TCH concentration of 100 mg L^{-1}. Therefore, as the initial TCH concentration increases, the degradation rate gradually decreases.[46] The decrease in the TCH degradation rate is mainly due to the competition of TCH molecules for the limited amounts of reactive species since the PMS concentration is fixed while the TCH concentration is increased. However, after one hour of reaction, the difference in degradation rate between different systems decreases, and the degradation rate can reach a good result. This result indicated that the method is suitable for a wide concentration range of TCH and could show a good removal effect, which was in good agreement with previous studies.[47]

3.3.5 Effect of initial solution pH. The initial pH value of the research solution is also one of the most significant factors that affect the degradation of TCH,[48] especially for reaction systems involving iron-based materials. Therefore, the effect of the initial pH on TCH degradation in the Fe_3O_4@T-BC/PMS system was studied, and the results are shown in Fig. 5e. The experiment was conducted at pH values of 3, 5, 7, 9 and 11. It was found that the degradation of TCH gradually increased with increasing pH. When pH = 3, the degradation is the lowest at 10 min, which is just 65.46%. It could be concluded that T-BC adsorbs a large amount of TCH, which makes it difficult for PMS to diffuse to the surface and pores of T-BC, thereby inhibiting the degradation of TCH. However, when pH = 11, the degradation reached 97.62% after 10 min, which was 1.5 times higher than that at pH = 3; moreover, it reached 99.86% after one hour of reaction. It was concluded that TCH is deprotonated in aqueous solution under alkaline conditions, so the degradation of TCH will increase and be more easily oxidized by $^{\bullet}OH$.[49] In addition, these findings were in good agreement with previous studies that alkaline conditions also have a good activation effect under the synergy of PMS. Moreover, it generated more $SO_4^{-\bullet}$, which further improved the degradation of TCH.[50] At the same time, at pH 10.0, in the reaction system without PMS, the degradation of TCH was just 13.86%. Thus, OH^- can activate PMS under alkaline conditions instead of alkali reacting directly with TCH, these results agree with previous studies reached a good agreement.[51] The reaction formula is as follows eqn (1) and (2):

$$2S_2O_8^{2-} + 2H_2O \rightarrow 3SO_4^{2-} + SO_4^{-\bullet} + {}^{\bullet}O_2^- + 4H^+ \quad (1)$$

$$SO_4^{-\bullet} + OH^- \rightarrow SO_4^{2-} + {}^{\bullet}OH \quad (2)$$

PMS will slowly self-decompose to produce $^1O_2$,[52] which is a highly selective oxidant and the main oxidation active material produced by activating PMS, but the reaction is extremely slow and the output of $^1O_2$ is extremely low according to Y. Qi.[53] However, under alkaline conditions, Fe_3O_4@T-BC-activated PMS accelerates the production of $^1O_2$ in the system; therefore, alkaline conditions can improve the degradation of TCH.

3.3.6 Effect of coexisting ions. Many inorganic anions often coexist in wastewater, which may affect the degradation process of pollutants. Fig. 5f shows the degradation of TCH in the Fe_3O_4@T-BC/PMS system in the presence of 50 mmol L^{-1} inorganic anions such as CO_3^{2-}, HCO_3^-, CH_3COO^-, Cl^-, and SO_4^{2-}. Among them, Cl^- showed little effect on the degradation in the first 15 minutes. However, it reduced the degradation because it is regarded as a scavenger of free radicals. The reaction will oxidize Cl^- to generate Cl_2 and $Cl_2^{-\bullet}$, and its reactivity is lower than that of $SO_4^{-\bullet}$ or $^{\bullet}OH$. These findings were in good agreement with previous studies.[54] HCO_3^-, CO_3^{2-} and CH_3COO^- can increase the pH, thereby promoting the activation of PMS and improving the degradation of TCH. Many studies have reported that although HCO_3^- is also a scavenger, the generated CO_3^{2-} also has a promoting effect.[55] In addition, PMS can oxidize HCO_3^- to produce a two-electron oxide HCO_4^-, which can promote the degradation of TCH. The reaction formula is as shown in eqn (3) and (4):

$$OH^- + HSO_5^- \rightarrow SO_5^{2-} + H_2O \quad (3)$$

$$SO_5^{2-} + HCO_3^- \rightarrow HCO_4^- + SO_4^{2-} \quad (4)$$

In addition, due to the effect of pH on the degradation efficiency of Fe_3O_4@T-BC-activated PMS, it can be seen that under alkaline conditions, it is more conducive to the degradation of TCH; thus, alkali ions can obviously promote the degradation of TCH. SO_4^{2-} has almost no effect on degradation; thus, it is inferred that SO_4^{2-} is not the main reactive species to degrade TCH.

3.3.7 Degradation kinetic analysis. Based on experience,[17] we have used pseudo first-order kinetics to fit the kinetic characteristics of TCH degradation in the Fe_3O_4@T-BC/PMS system (eqn (5)).

$$-\ln(C_t/C_0) = kt \quad (5)$$

Fig. 5g shows the fitting results of pseudo-first-order kinetics of its degradation rate under different TCH concentrations. It can be seen from the figure that when the TCH concentration is 25 mg L^{-1}, 50 mg L^{-1}, 75 mg L^{-1}, 100 mg L^{-1}, the pseudo first-order degradation rate (the slope of the curve) is respectively 0.0224 min^{-1}, 0.0234 min^{-1}, 0.0249 min^{-1}, 0.0252 min^{-1}. Within a certain range, the degradation rate of TCH in the system increases with the increase of its concentration.

3.4 Reaction mechanisms

3.4.1 Mechanism of Fe_3O_4@T-BC for TCH adsorption. In order to further study the role of composite materials in the process of activating PMS to remove TCH, combined with the existing adsorption experiment experience,[56,57] the following experiment was designed: add 0.025 g, 0.05 g, 0.1 g, 0.15 g, 0.2 g, 0.25 g, 0.3 g Fe_3O_4@T-BC to 25 mg L^{-1} TCH, and keep shaking at room temperature to promote its full adsorption until the concentration of TCH no longer decreases. According to the experimental results, draw the adsorption isotherm as shown in Fig. 6. The results show that the adsorption effect of Fe_3O_4@T-

 © 2021 The Author(s). Published by the Royal Society of Chemistry

Open Access Article. Published on 22 May 2021. Downloaded on 12/5/2025 7:07:59 PM.
This article is licensed under a Creative Commons Attribution-NonCommercial 3.0 Unported Licence.

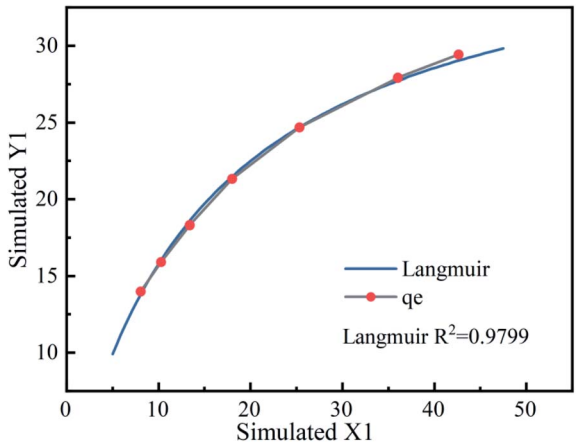

Fig. 6 Adsorption isotherm of Fe_3O_4@T-BC to TCH.

BC on TCH is L-type adsorption. It can be inferred from FT-IR that Fe_3O_4@T-BC has abundant oxygen-containing functional groups on the surface, which increase the adsorption sites on the surface of biochar and promote the degradation process of PMS.[14] Therefore, we believe that the excellent adsorption performance of the composite material can be attributed not only to the porous structure of the surface, but also to the chemical adsorption and electrostatic adsorption caused by the oxygen-containing groups on the surface of the oxidized biochar. At the same time, these oxygen-containing groups increases the catalytic activity of activated PMS, produce more free radicals, further improving the degradation of TCH.[53]

3.4.2 Identification and generation mechanism of the dominant radicals. We conducted an investigation on the mechanism of free radical production. As reported, free radicals, including $SO_4^{-\bullet}$, $^\bullet OH$, $^\bullet O_2^-$ and $^1O_2$, were the primary reactive oxygen species (ROS) in the metal@carbon/PMS system.[58] The presence of the above ROS in the Fe_3O_4@T-BC/PMS system was confirmed by EPR characterization. DMPO and TEMP were used as spin trapping agents for the determination of $SO_4^{-\bullet}$, $^\bullet OH$, $^\bullet O_2^-$ and $^1O_2$. As shown in Fig. 7a, add DMPO to the system, after 10 min of reaction, the signal of DMPO–$^\bullet O_2^-$ (1 : 1 : 1 : 1 DMPO–$^\bullet O_2^-$ characteristic peak) adducts can be found, indicating the presence of $^\bullet O_2^-$ in the system. Then, TEMP was added to another system, as shown in Fig. 7b, and the TEMP–$^1O_2$ characteristic peak with an intensity ratio of 1 : 1 : 1 appeared, indicating that $^1O_2$ also participated in the catalytic reaction. And the characteristic signal of DMPO–$^\bullet OH$ and DMPO–$SO_4^{-\bullet}$ adducts appeared in the Fe_3O_4@T-BC/PMS system (the 1 : 2 : 2 : 1 DMPO–$^\bullet OH$ characteristic peak, the 1 : 1 : 1 : 1 : 1 : 1 DMPO–$SO_4^{-\bullet}$ characteristic peak), as shown in Fig. 7c. Therefore, $^\bullet OH$ and $SO_4^{-\bullet}$ were also involved in the catalytic oxidation reaction.

To further study the effect of free radicals in the Fe_3O_4@T-BC/PMS system on the degradation efficiency, quenching experiments were conducted to identify the dominant reactive radicals in the Fe_3O_4@T-BC/PMS system. Herein, EtOH was used to quench both $SO_4^{-\bullet}$ ($k_{SO_4^{-\bullet}} = (1.6–7.7) \times 10^7$/M s) and $^\bullet OH$ ($k_{\cdot OH} = (1.2–2.8) \times 10^9$/M s).[21] TBA was used to quench $^\bullet OH$ ($k_{\cdot OH} = (3.8–7.6) \times 10^8$/M s).[22] FFA was used to quench $^1O_2$ ($k_{^1O_2} = 1.2 \times 10^8$/M s).[23] *p*-BQ was used to quench $^\bullet O_2^-$.[24] Under the same conditions, the lower the degradation rate, the more obvious the inhibitory effect, and the greater the influence of the free radicals on the degradation reaction. As shown in Fig. 8a, the degradation rate of TCH in the blank control group reached 91.98% after 60 minutes, while the degradation rate of TCH was inhibited to varying degrees after adding the quencher, indicating that all four free radicals exist in the reaction system and play a role in the degradation process effect.[59] Among them, the most obvious decline in the degradation rate of TCH was in the FFA-$^1O_2$ group (Fig. 8b); within 60 minutes of the reaction, the degradation rate of TCH in the FFA-$^1O_2$ group was always the lowest, and the reaction speed was the slowest. Therefore, $^1O_2$ is an important ROS in the degradation process of TCH. It is worth noting that the inhibitory effect of *p*-BQ on TCH degradation is significantly weaker than that of FFA, indicating that $^\bullet O_2^-$ is not the only precursor to generate $^1O_2$ in the Fe_3O_4@T-BC/PMS system.[23,60,61]

The production of active free radicals in the Fe_3O_4@T-BC/PMS system is affected by the dissolution efficiency of iron ions. According to the experimental results, Fe^{3+} is the main iron ion in the system. Fig. 8c reflects the changes in different valence iron ions in the solution during the degradation process. First, Fe^{3+} reacts with PMS to form Fe^{2+} and $SO_5^{-\bullet}$. PMS can cause Fe^{2+} to lose electrons to form Fe^{3+} and produce $SO_4^{-\bullet}$, which can degrade target organic pollutants. It is speculated that the possible reaction process on the catalyst surface is as follows:[62,63]

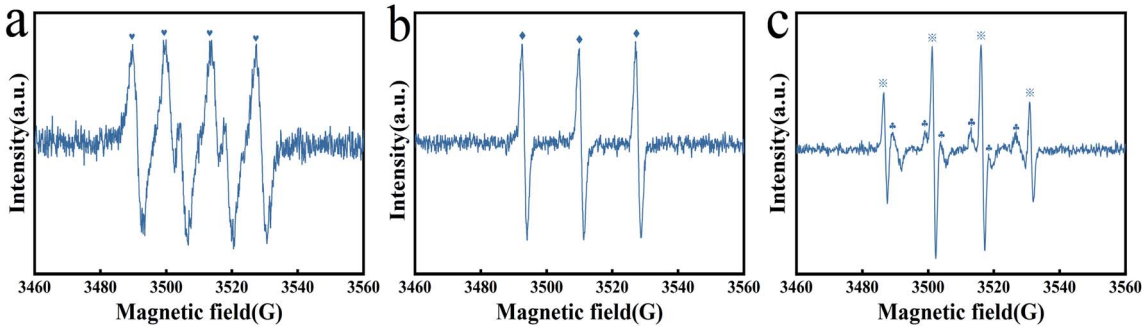

Fig. 7 EPR spectra of $^\bullet O_2^-$ (a), $^1O_2$ (b), $SO_4^{-\bullet}$ and $^\bullet OH$ (c).

Open Access Article. Published on 22 May 2021. Downloaded on 12/5/2025 7:07:59 PM.
This article is licensed under a Creative Commons Attribution-NonCommercial 3.0 Unported Licence.

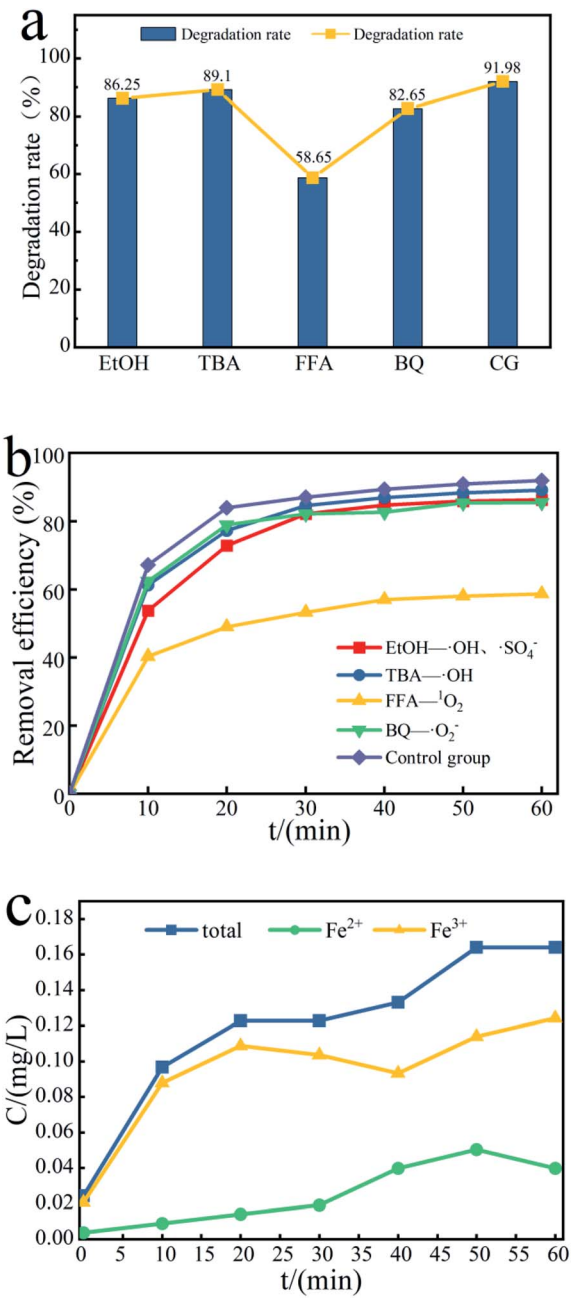

Fig. 8 (a) Effect of free radical scavengers on TCH removal efficiency, and (b) the contribution of $SO_4^{-\bullet}$, $^\bullet OH$, $^\bullet O_2^-$ and $^1O_2$; (c) concentration changes of iron ions in different valence states.

Within 10–20 minutes of reaction, the concentration of Fe^{3+} decreases and the concentration of Fe^{2+} increases:

$$Fe^{3+} + HSO_5^- \rightarrow Fe^{2+} + SO_5^{-\bullet} + H^+ \quad (6)$$

Within 50–60 min of the reaction, the concentration of Fe^{2+} decreases and the concentration of Fe^{3+} increases:

$$Fe^{2+} + HSO_5^- \rightarrow Fe^{3+} + SO_4^{-\bullet} + OH^- \quad (7)$$

As the reaction progresses, the concentration of iron ions in the solution changes only to a small extent (on the order of 0.1 mg L^{-1}). Compared to directly adding metal catalysts to the solution, the loading method effectively reduces the concentration of iron ions in the solution and avoids secondary pollution.

The results of the abovementioned investigation on iron ions explain the production of $SO_4^{-\bullet}$ (8) and (9).[62] At the same time, Fe^{2+} interacts with the dissolved oxygen in the system to produce $^\bullet O_2^-$ (10).[64] The generated $SO_4^{-\bullet}$ reacts with water to produce $^\bullet OH$ (11). $^\bullet O_2^-$ can react with H_2O and $^\bullet OH$ to generate $^1O_2$ (12) and (13). It is speculated from the results of the quenching experiment that $^\bullet O_2^-$ is not the only way to produce $^1O_2$; the data show that $SO_5^{-\bullet}$ produced by Fe^{3+} and HSO_5^- can also act to produce $^1O_2$ (14) and (15).[23] Finally, the combined action of several free radicals completes the degradation of TCH (16).[65,66]

$$Fe^{3+} + HSO_5^- \rightarrow Fe^{2+} + SO_5^{-\bullet} + H^+ \quad (8)$$

$$Fe^{2+} + HSO_5^- \rightarrow Fe^{3+} + SO_4^{-\bullet} + OH^- \quad (9)$$

$$Fe^{2+} + O_2 \rightarrow Fe^{3+} + {}^\bullet O_2^- \quad (10)$$

$$SO_4^{-\bullet} + H_2O \rightarrow SO_4^{2-} + {}^\bullet OH + H^+ \quad (11)$$

$$2{}^\bullet O_2^- + H_2O \rightarrow H_2O_2 + OH^- + {}^1O_2 \quad (12)$$

$${}^\bullet O_2^- + {}^\bullet OH + 2H^+ \rightarrow {}^1O_2 + OH^- \quad (13)$$

$$SO_5^{-\bullet} + SO_5^{-\bullet} \rightarrow S_2O_8^{2-} + {}^1O_2 \quad (14)$$

$$SO_5^{-\bullet} + SO_5^{-\bullet} \rightarrow SO_4^{2-} + {}^1O_2 \quad (15)$$

$$TCH + SO_4^{-\bullet} + {}^\bullet OH + {}^\bullet O_2^- + {}^1O_2 \rightarrow \text{intermediates} + CO_2 + H_2O \quad (16)$$

In the above process, the sources of $^1O_2$ are the most diverse and play a major role in the degradation system.

3.4.3 Degradation mechanisms. TCH contains a conjugated system composed of a benzene ring, ketone group and

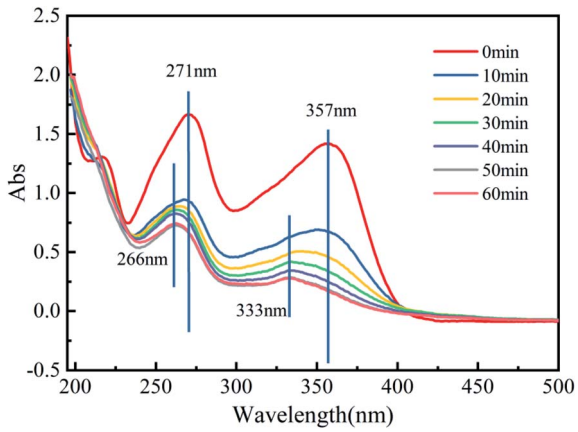

Fig. 9 UV-Vis spectra of TCH in the Fe_3O_4@T-BC/PMS system.

 © 2021 The Author(s). Published by the Royal Society of Chemistry

Open Access Article. Published on 22 May 2021. Downloaded on 12/5/2025 7:07:59 PM.
This article is licensed under a Creative Commons Attribution-NonCommercial 3.0 Unported Licence.

enol, and its structure has 2 chromophoric groups.[67] Fig. 9 reflects the variation in the UV-Vis spectrum with reaction time in the Fe_3O_4@T-BC/PMS system. The two main peaks (271 nm and 357 nm) correspond to four different ring structures in the molecular structure. After the reaction started, the two characteristic peaks decreased rapidly with increasing reaction time and blueshifted. The above results indicate that the benzene ring structure is continuously cleaved. These first occur at the unsaturated bond position of the benzene ring, and then the benzene ring generates a series of small molecular intermediate products through ring opening and oxidation. This is consistent with previous research.[16]

In order to further analyze the intermediate products and infer the degradation path of tetracycline, the degradation products of tetracycline were analyzed by LC-MS. 8 kinds of intermediates in the degradation process are detected, and the possible TCH degradation pathways are proposed (Fig. 10). TCH is first decomposed into tetracycline, and the initial m/z value of the original TC was 445. Through the attack of $SO_4^{-\bullet}$, $^{\bullet}OH$, $^{\bullet}O_2^-$ and $^1O_2$, the oxidation of TC may occur in three ways. In both route I and route II, intermediate product F is formed. In route I, $^{\bullet}OH$ first attacked the double bond on the c ring to form product A ($m/z = 461$), $^{\bullet}OH$ attacked the double bond on the d ring of product A again, and produced products D ($m/z = 479$), E ($m/z = 477$). The dimethylamino group of the product E is attacked by $SO_4^{-\bullet}$, $^1O_2$, and the aromatic epoxide is oxidized to open the ring, and the product F is obtained. In route II, a epoxidation opens the ring, the c-ring double bond is attacked by $^{\bullet}OH$, and the dimethylamino group is hydroxylated to produce product B ($m/z = 483$). The d-ring hydroxyl group in product B is oxidized to carbonyl by $^1O_2$.[64] The product F ($m/z = 495$) was obtained. The product F eliminates the amide group to obtain the intermediate product G ($m/z = 451$).[22] In route III, the D-ring double bond undergoes a hydrolysis reaction, and the dimethylamino group is demethylated to produce the product C ($m/z = 436$). Product C obtains intermediate product H ($m/z = 314$) through a series of reactions (dehydration, addition and oxidation). Finally, under the continued attack of the four free radicals, these intermediate products undergo a ring-opening reaction, and finally mineralize into NH_4^+, NO_3^-, CO_2 and H_2O.

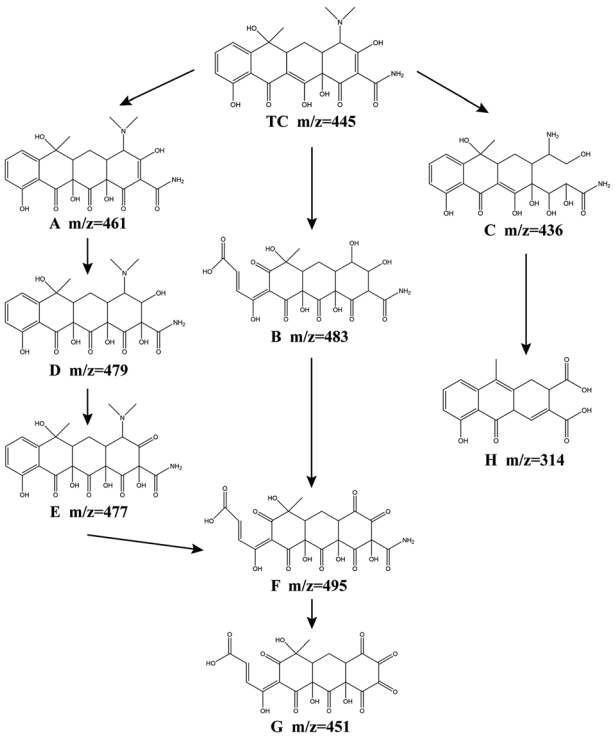

Fig. 10 TCH degradation pathways in the Fe_3O_4@T-BC/PMS system.

3.4.4 Mineralization of TCH. The ultimate goal is to achieve degradation experiments mineralization of organic matter, and only a higher degradation rate cannot be expressed sufficiently effectively degradation of the substrate. The reason is that, in some cases, the degradation of the system only breaks some of the chemical bonds of organics to produce long-chain molecular organics, and these organics may be reconnected under appropriate conditions, which will form new organic pollutants. New pollutants cannot be reflected in the detection of target pollutants, but they still pose a threat to the environment. Therefore, TOC detection is a powerful data support to determine the effect of degradation experiments.[68]

Fig. 11 shows that the treatment system can mineralize part of TCH into CO_2 and H_2O in a short time. After treating TCH with PMS activated by 1 g L^{-1} Fe_3O_4@T-BC, the TOC content in the system decreased. To verify the system's mineralization of TCH and the intermediate products produced by its degradation. A degradation experiment of 270 min was carried out (experimental conditions: 2 g L^{-1} PMS, 50 mg L^{-1} TCH, 2 g L^{-1} Fe_3O_4@T-BC, room temperature). The TOC change during the experiment is shown in the figure. In the first 60 min of the degradation experiment, the TOC value decreased rapidly, consistent with the TCH degradation efficiency; after 60 minutes of the experiment, the TOC value decreased gradually. It can be inferred from this that Fe_3O_4@T-BC effectively catalyzes the generation of a large number of active free radicals in the initial stage of degradation. These free radicals further oxidize the intermediate products of TCH degradation, attack

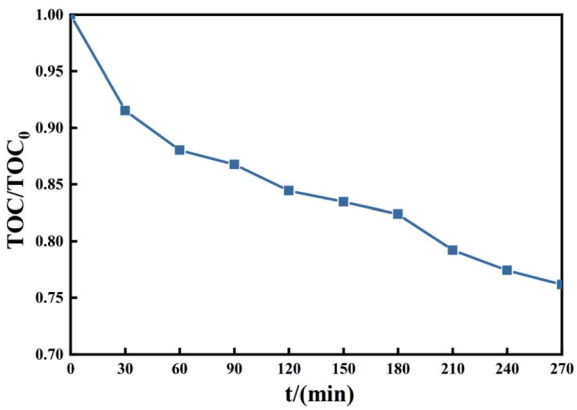

Fig. 11 The change of TOC during TCH degradation in the Fe_3O_4@T-BC/PMS system.

Open Access Article. Published on 22 May 2021. Downloaded on 12/5/2025 7:07:59 PM.
This article is licensed under a Creative Commons Attribution-NonCommercial 3.0 Unported Licence.

higher bond energy chemical bonds, and finally mineralize TCH into CO_2 and H_2O.

3.5 Stability and reusability of Fe_3O_4@T-BC

To evaluate the stability of the catalyst in the activated persulfate system and the possibility of repeated use, the stability of Fe_3O_4@T-BC was evaluated in a cyclic degradation test under optimal conditions, and the results are shown in Fig. 12. Four repeated experiments were carried out with 60 min as a reaction cycle, and the conditions for each test were controlled as follows: [TCH] = 50 mg L^{-1}, Fe_3O_4@T-BC dosage = 1 g L^{-1}, [PMS] = 1 g L^{-1}. After the previous reaction cycle, an external magnet is used to recover and separate the magnetic catalyst (Fig. 3b), and washed repeatedly with ultrapure water until neutral pH was achieved, dried at 60 °C and weighed. Then, the degradation experiment was performed again under the same conditions. As shown in Fig. 12, the degradation efficiency of TCH gradually decreases as the number of cycles increases. It was found by weighing that there was a mass loss of approximately 10% in each round of catalyst recovery. The loss of the catalyst mainly includes the external magnetic field residue and a small part of Fe_3O_4 detached during the washing process of deionized water. In general, the Fe_3O_4@T-BC catalyst can still maintain a degradation rate of 71.32% after repeating the degradation experiment 4 times, indicating that the Fe_3O_4@T-BC catalyst is stable and can be recycled in the PMS activation of TCH degradation. In addition, for each cycle experiment, the leaching of total iron was less than 0.2 ppm, which is lower than the European standard (2 ppm).[14] Fig. 2a also shows that there is no significant difference in the XRD patterns of the Fe_3O_4@T-BC catalyst before and after the reaction. Fe_3O_4@T-BC is easily separated and reused by an external magnetic field, indicating that the catalyst has high practical application value. In addition, cost accounting was carried out. Under the experimental conditions, the production of T-BC per ton of tea residue is about 700 kg. Through calculation, the electricity cost per ton for preparing T-BC is 1528.7 yuan, and the equipment depreciation is 7 yuan, totaling 1535.7 yuan. According to the market price of activated carbon, it is 10 000–15 000 yuan per ton. It can be seen from the above conditions that the cost of tea residue biochar is much lower than the average price of activated carbon. Considering that the raw materials for preparing Fe_3O_4@T-BC are widely available and low in price, the material can be used as a stable and promising composite material.

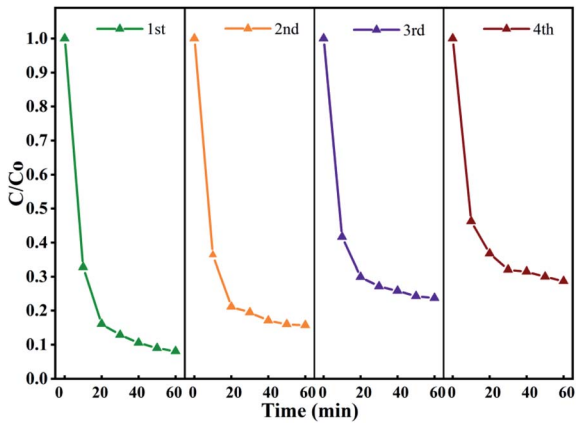

Fig. 12 Stability and reusability of Fe_3O_4@T-BC for TCH degradation in the Fe_3O_4@T-BC/PMS system.

4. Conclusions

In this study, the strategy of converting tea residue waste into biochar and loading Fe_3O_4 as the activator of PMS was realized for the first time, achieving waste recycling with low cost. Under the optimal reaction conditions, the removal rate of TCH within 60 minutes can reach 97.89%, which has extremely high degradation efficiency. Also, the strategy, loading Fe_3O_4 with catalytic properties on the biochar material to synergistically catalyze the PMS oxidative degradation of TCH, can solve the problem of the low activation effect of a single biochar and the problem of secondary pollution caused by the leaching of iron ions when a single iron activates PMS. The magnetic properties of the catalyst material are used for recycling, which has the huge potential for practical application. The mechanism of TCH degradation in the Fe_3O_4@T-BC/PMS system includes free radical and nonradical pathways, $SO_4^{-\bullet}$ and $^1O_2$ played a dominant role. It is comprehensively shows that Fe_3O_4@T-BC is a promising magnetic biochar-based composite material that is economical, efficient, and environmentally friendly while realizing the reuse of waste resources. Therefore, the activation technology is expected to be further promoted for treat other types of antibiotic pollutants and even other organic pollutants.

Conflicts of interest

There are no conflicts to declare.

Acknowledgements

This work was supported by National Undergraduate Training Program for Innovation and Entrepreneurship (201910225066; 202010225090), and the Heilongjiang Provincial Natural Science Foundation (LH2019D002).

References

1 B. Mohammad, T. Targol, K. Elaheh and E. Ali, *Mater. Circ. Econ.*, 2021, **3**, 3.
2 Q. Xu, K. Hu, X. Wang, D. Wang and M. T. Knudsen, *J. Cleaner Prod.*, 2019, **233**, 782–792.
3 B. Li, Y. Mei and S. Fan, *Environ. Sci. Technol.*, 2020, **43**(9), 67–78.
4 V. Basumatary, R. Saikia, R. Narzari, N. Bordoloi, L. Gogoi, D. Sut, N. Bhuyan and R. Kataki, *Mater. Today: Proc.*, 2018, **5**(11), 23413–23422.
5 B. Shen, L. Tian, F. Li, X. Zhang, H. Xu and S. Singh, *Fuel*, 2017, **187**, 189–196.
6 H. Qiao, L. Mei, G. Chen, H. Liu, C. Peng, F. Ke, R. Hou, X. Wan and H. Cai, *Appl. Surf. Sci.*, 2019, **483**, 114–122.

 © 2021 The Author(s). Published by the Royal Society of Chemistry

Open Access Article. Published on 22 May 2021. Downloaded on 12/5/2025 7:07:59 PM.
This article is licensed under a Creative Commons Attribution-NonCommercial 3.0 Unported Licence.

7 S. Fan, W. Liu, J. Wang, H. Hu and N. Zhou, *Environ. Sci.*, 2020, **41**(3), 1308–1318.
8 I. T. Carvalho and L. Santos, *Environ. Int.*, 2016, **94**, 736–757.
9 M. Bilal, S. Mehmood, T. Rasheed and H. M. N. Iqbal, *Curr. Opin. Environ. Sci. & Health*, 2020, **13**, 68–74.
10 L. Xu, H. Zhang, P. Xiong, Q. Zhu, C. Liao and G. Jiang, *Sci. Total Environ.*, 2020, **753**, 141975.
11 H. Wang, X. Lou, Q. Hu and T. Sun, *J. Mol. Liq.*, 2021, **325**, 114967.
12 G. Sharma, A. Kumar, S. Sharma, A. H. A. Muhtaseb, M. Naushad, A. Ghfar, T. Ahamad and F. J. Stadler, *Sep. Purif. Technol.*, 2019, **211**, 895–908.
13 G. Sharma, D. Dionysiou, S. Sharma, A. Kumar, A. H. A. Muhtaseb, M. Naushad and F. J. Stadler, *Catal. Today*, 2019, **335**, 437–451.
14 Z. Pi, X. Li, D. Wang, Q. Xu, Z. Tao, X. Huang, F. Yao, Y. Wu, L. He and Q. Yang, *J. Cleaner Prod.*, 2019, **235**, 1103–1115.
15 H. Chao, D. E. Que, A. C. Aquino, Y. Gou, L. Tayo, Y. Lin, M. Tsai, F. Hsu, I. Lu, S. Lin, N. Srikhao, C. Shy and K. Huang, *Environ. Monit. Assess.*, 2020, **192**, 220–229.
16 F. Shao, Y. Wang, Y. Mao, T. Shao and J. Shang, *Chemosphere*, 2020, **261**, 127844.
17 P. Xiao, L. An and D. Wu, *N. Carbon Mater.*, 2020, **35**, 667–683.
18 K. Zhu, Q. Bin, Y. Shen, J. Huang, D. He and W. Chen, *Chem. Eng. J.*, 2020, **402**, 126090.
19 L. An and P. Xiao, *RSC Adv.*, 2020, **10**, 19401–19409.
20 D. Ouyang, J. Yan, L. Qian, Y. Chen, L. Han, A. Su, W. Zhang, H. Ni and M. Chen, *Chemosphere*, 2017, **184**, 609–617.
21 S. Shao, L. Qian, X. Zhan, M. Wang, K. Lu, J. Peng, D. Miao and S. Gao, *Chem. Eng. J.*, 2020, **382**, 123005.
22 X. Chen, J. Zhou, Y. Chen, Y. Zhou and X. Li, *Process Saf. Environ. Prot.*, 2020, **145**, 346–377.
23 Y. Yan, H. Zhang, W. Wang, W. Li, Y. Ren and X. Li, *J. Hazard. Mater.*, 2020, **411**, 124952.
24 Z. Li, K. Li, S. Ma, B. Dang and Q. Meng, *J. Colloid Interface Sci.*, 2020, **582**, 598–609.
25 K. Mahesh, D. Kuo and B. Huang, *J. Mol. Catal. A: Chem.*, 2015, **396**, 290–296.
26 R. Gurav, S. Bhatia, T. Choi, Y. Park, J. Park, Y. Han, G. Vyavahare, J. Jadhav, J. Song, P. Yang, J. Yoon, A. Bhatnagar, Y. Choi and Y. Yang, *Bioresour. Technol.*, 2019, **297**, 122472.
27 B. Chen, Z. Chen and S. Lv, *Bioresour. Technol.*, 2011, **102**(2), 716–723.
28 A. Kumar, G. Sharma, M. Naushad, A. H. Al-Muhtaseb, A. Kumar, I. Hira, T. Ahamad, A. A. Ghfar and F. J. Stadler, *J. Environ. Manage.*, 2019, **231**, 1164–1175.
29 G. Sharma, S. Bhogal, V. K. Gupta, S. Agarwal, A. Kumar, D. Pathania, G. T. Mola and F. J. Stadler, *J. Mol. Liq.*, 2019, **275**, 499–509.
30 J. Hoslett, H. Ghazal, E. Katsou and H. Jouhara, *Sci. Total Environ.*, 2021, **751**, 141755.
31 X. Duan, H. Sun, J. Kang, Y. Wang, S. Indrawirawan and S. Wang, *ACS Catal.*, 2015, **5**, 4629–4636.
32 J. Yan, L. Han, W. Gao, S. Xue and M. Chen, *Bioresour. Technol.*, 2015, **175**, 269–274.
33 W. Oh, Z. Dong and T. Lim, *Appl. Catal., B*, 2016, **218**, 77–83.
34 Z. Ma, Y. Guan and H. Liu, *J. Polym. Sci., Part A: Polym. Chem.*, 2005, **43**(15), 3433–3439.
35 B. Li, Y. Zhang, J. Xu, Y. Mei, S. Fan and H. Xu, *Chemosphere*, 2020, **267**, 129283.
36 Y. Lei, C. Chen, Y. Tu, Y. Huang and H. Zhang, *Environ. Sci. Technol.*, 2015, **49**, 6838–6845.
37 J. Wang, Z. Liao, J. Ifthikar, L. Shi, Y. Du, J. Zhu and Z. Chen, *Chemosphere*, 2017, **185**, 754–763.
38 Y. Du, M. Dai, J. Cao and C. Peng, *RSC Adv.*, 2019, **9**, 33486–33496.
39 P. Duan, Y. Qi, S. Feng, X. Peng, W. Wang, Y. Yue, Y. Shang, Y. Li, B. Gao and X. Xu, *Appl. Catal., B*, 2020, **267**, 118717.
40 D. Ma, Y. Yang, B. Liu, G. Xie, C. Chen, N. Ren and D. Xing, *Chem. Eng. J.*, 2021, **408**, 127992.
41 L. Hou, X. Li, Q. Yang, F. Chen, S. Wang, Y. Ma, Y. Wu, X. Zhu, X. Huang and D. Wang, *Sci. Total Environ.*, 2019, **663**, 453–464.
42 Y. Ji, C. Dong, D. Kong, J. Lu and Q. Zhou, *Chem. Eng. J.*, 2015, **263**, 45–54.
43 Z. Li, C. Guo, J. Lu, Z. Hu and M. Ge, *J. Hazard. Mater.*, 2019, **373**, 85–96.
44 S. Luo, P. Qin, J. Shao, L. Peng, Q. Zeng and J. Gu, *Chem. Eng. J.*, 2013, **223**, 1–7.
45 C. Zhu, G. Fang, D. Dionysiou, C. Liu, J. Gao, W. Qin and D. Zhou, *J. Hazard. Mater.*, 2016, **316**, 232–241.
46 A. Ioannidi, P. Oulego, S. Collado, A. Petala, V. Arniella, Z. Frontistis, G. N. Angelopoulos, M. Diaz and D. Mantzavinos, *J. Environ. Manage.*, 2020, **270**, 110820.
47 F. Li, F. Duan, W. Ji and X. Gui, *Ecotoxicol. Environ. Saf.*, 2020, **198**, 110653.
48 M. Nalinrut, R. Chavalit and M. Lu, *Environ. Sci. Technol.*, 2009, **43**(22), 8629–8634.
49 W. Zhai, M. Li and Q. Zhang, *China Environ. Sci.*, 2020, **40**(6), 2483–2492.
50 Y. Guan, J. Ma, X. Li, J. Fang and L. Chen, *Environ. Sci. Technol.*, 2011, **45**(21), 9308–9314.
51 S. Yao, X. Ma and S. Li, *China Environ. Sci.*, 2018, **38**(11), 4166–4172.
52 Z. Guo, G. Bai, B. Huang, N. Cai, P. Guo and L. Chen, *J. Hazard. Mater.*, 2021, **408**, 124802.
53 Y. Qi, B. Ge, Y. Zhang, B. Jiang, C. Wang, M. Akram and X. Xu, *J. Hazard. Mater.*, 2020, **399**, 123039.
54 Y. Yang, P. Joseph J, J. Ma and M. William A, *Environ. Sci. Technol.*, 2014, **48**(4), 2344–2351.
55 Y. Wang, D. Tian, W. Chu, M. Li and X. Lu, *Sep. Purif. Technol.*, 2019, **212**, 536–544.
56 S. Gaurav, K. Amit, N. Mu, G. Alberto, A. Ala'a H, A. Ayman, S. Vikrant, A. Tansir and J. Florian, *Int. J. Biol. Macromol.*, 2018, **114**, 295–305.
57 S. Gaurav, K. Amit, D. Kunjana, S. Shweta, N. Mu, A. Ayman, A. Tansir and J. Florian, *Carbohydr. Polym.*, 2018, **202**, 444–453.
58 K. Mona, M. Gholamreza and G. Stefanos, *Chem. Eng. J.*, 2020, **411**, 127957.
59 F. Liu, J. Cao, Z. Yang, W. Xiong and X. Zhong, *J. Colloid Interface Sci.*, 2020, **581**, 195–204.

Open Access Article. Published on 22 May 2021. Downloaded on 12/5/2025 7:07:59 PM.
This article is licensed under a Creative Commons Attribution-NonCommercial 3.0 Unported Licence.

60 X. Li, T. Hou, L. Yan, L. Shan and Y. Zhao, *J. Hazard. Mater.*, 2020, **398**, 122884.
61 Y. Shi, J. Li, D. Wan, J. Huang and Y. Liu, *Sci. Total Environ.*, 2020, **749**, 142313.
62 J. Hu, H. Chen, H. Dong, L. Zhu and J. Yu, *J. Hazard. Mater.*, 2020, **403**, 123553.
63 Q. Hu, J. Cao, Z. Yang, W. Xiong, Z. Xu, P. Song, M. Jia, Y. Zhang, H. Peng and A. Wu, *Sep. Purif. Technol.*, 2020, **259**, 118059.
64 H. Huang, T. Guo, K. Wang, Y. Li and G. Zhang, *Sci. Total Environ.*, 2021, **758**, 143957.
65 R. Zhang, D. Li, J. Sun, Y. Cui and Y. Sun, *Front. Environ. Sci. Eng.*, 2020, **14**(4), 6955–6960.
66 M. Shen, Z. Huang, L. Qiu, Z. Chen and L. Cui, *J. Cleaner Prod.*, 2020, **268**, 122174.
67 B. Yu, J. Wang and X. Yang, *Environ. Sci. Pollut. Res.*, 2019, **26**, 32345–32359.
68 C. Zhao, S. Zhong, C. Li, H. Zhou and S. Zhang, *J. Mater. Res. Technol.*, 2020, **9**(1), 601–609.

 © 2021 The Author(s). Published by the Royal Society of Chemistry